

# Wave Functions of the Proton Ground State in the Presence of a Uniform Background Magnetic Field in Lattice QCD

Dale S. Roberts,<sup>1</sup> Patrick O. Bowman,<sup>2</sup> Waseem Kamleh,<sup>1</sup> and Derek B. Leinweber<sup>1</sup>

<sup>1</sup>*Special Research Centre for the Subatomic Structure of Matter  
and Department of Physics, University of Adelaide 5005, Australia.*

<sup>2</sup>*Centre for Theoretical Chemistry and Physics and Institute of Natural Sciences,  
Massey University (Albany), Private Bag 102904, North Shore City 0745, New Zealand*

We calculate the probability distributions of quarks in the ground state of the proton, and how they are affected in the presence of a constant background magnetic field. We focus on wave functions in the Landau and Coulomb gauges. We observe the formation of a scalar  $u$ - $d$  diquark clustering. The overall distortion of the quark probability distribution under a very large magnetic field, as demanded by the quantisation conditions on the field, is quite small. The effect is to elongate the distributions along the external field axis while localizing the remainder of the distribution.

PACS numbers: 12.38.Gc, 12.38.Aw, 14.20.Dh

## I. INTRODUCTION

The wave function of a baryon on the lattice provides insight into the shape and properties of the particle. Furthermore, the wave function also provides a diagnostic tool for the lattice, being able to determine how well a particular state fits on the lattice volume. The earliest work on wave functions on the lattice was carried out on small lattices, for the pion and rho, initially in  $SU(2)$  [1]. Further progress was made in the early nineties, where gauge invariant Bethe-Salpeter amplitudes were constructed for the pion and rho [2, 3] by choosing a path ordered set of links between the quarks. This was then used to qualitatively show Lorentz contraction in a moving pion. Hecht and DeGrand [4] conducted an investigation on the wave functions of the pion, rho, nucleon and Delta using a gauge dependent form of the Bethe-Salpeter amplitude, primarily focusing on the Coulomb gauge.

The background field method [5] for placing an external electromagnetic field on the lattice has been used extensively in lattice QCD to determine the magnetic moments of hadrons. Early studies on very small lattices with only a few configurations [6, 7] showed remarkable agreement with the experimental values of the magnetic moments of the proton and neutron. More recent studies on magnetic moments [8] have shown good agreement with experimental values of the magnetic moments of the baryon octet and decuplet. This method has also been extended to the calculation of magnetic and electric polarisabilities [9, 10]. Here we use the wave function to determine the effect of the background magnetic fields on the shape of the proton.

As background field methods have become more widely used, it is apparent that the large fields demanded by the quantisation conditions should cause some concern with regards to the calculation of moments and polarisabilities. It is entirely possible that the distortion caused by these fields could be so dramatic that the particle under investigation bears little resemblance to its zero-field

form. For this reason, we will use the wave function as a tool to investigate the deformation caused by a background field on a particle.

## II. WAVE FUNCTION OPERATORS

The wave function of a baryon on the lattice is defined to be proportional to the two-point correlation function at zero momentum in position space. The two-point correlation function in position space for a proton can be written as

$$G(\vec{x}, t) = \langle \Omega | T \{ \chi_P(x) \bar{\chi}_P(0) \} | \Omega \rangle, \quad (1)$$

where the Dirac indices have been suppressed. The operators  $\bar{\chi}_P$  and  $\chi_P$  create and annihilate the proton respectively.  $\chi_P$  is given by

$$\chi_P(\vec{x}) = \epsilon^{abc} (u_a^T(\vec{x}) C \gamma_5 d_b(\vec{x})) u_c(\vec{x}), \quad (2)$$

where  $u$  and  $d$  are the Dirac spinors for the up quark and down quark respectively and  $C = \gamma_2 \gamma_4$  is the charge conjugation matrix in the Pauli representation, with Dirac indices suppressed and colour indices present. This interpolating field is chosen as it couples strongly to the ground state of the proton. From this, we construct the adjoint spinor that will create the proton:

$$\begin{aligned} \bar{\chi}_P(\vec{x}) &= \chi_P^\dagger \gamma_0 \\ &= \epsilon^{abc} \bar{u}_a(\vec{x}) (\bar{d}_b(\vec{x}) C \gamma_5 \bar{u}_c^T(\vec{x})). \end{aligned} \quad (3)$$

In order to construct the wave function across the entire lattice, we need to modify the definition of the annihilation operator to be able to annihilate each of the quarks at different points on the lattice with respect to some central point or origin. In this case, we wish to have two quarks annihilate some distance in one dimension from  $\vec{x}$  and have the remaining quark annihilate at any other point on the lattice with respect to  $\vec{x}$ . This gives

$$\chi_P(\vec{x}, \vec{y}, \vec{z}, \vec{w}) = \epsilon^{abc} (u_a^T(\vec{x} + \vec{y}) C \gamma_5 d_b(\vec{x} + \vec{z})) u_c(\vec{x} + \vec{w}). \quad (4)$$

For the case of a  $d$  quark wave function, we select  $\vec{w} = (d_1, 0, 0)$  and  $\vec{y} = (d_2, 0, 0)$ . For separations of the  $u$  quarks across even numbers of lattice sites,  $d_1 = -d_2$ , and for odd separations,  $d_1 + 1 = -d_2$ . We consider eight values for the separation of the quarks in Eq (5), between 0 and 7 lattice spacings, or 0 fm to 0.896 fm.

Wave functions of the  $u$  quarks are explored in a similar manner. By inserting this into the definition of the two-point correlation function in Eq. (1) and restoring Dirac indices, we arrive at the definition of the wave function operator

$$\begin{aligned}
G_{\gamma\delta}(\vec{x}, \vec{y}, \vec{z}, \vec{w}, t) &= \epsilon^{abc} \epsilon^{a'b'c'} (C\gamma_5)_{\alpha\beta} (C\gamma_5)_{\mu\nu} \langle \Omega | u_\alpha^a(\vec{x} + \vec{y}) d_\beta^b(\vec{x} + \vec{z}) u_\gamma^c(\vec{x} + \vec{w}) \bar{u}_\delta^{a'}(0) \bar{d}_\mu^{b'}(0) \bar{u}_\nu^{c'}(0) | \Omega \rangle \\
&= -\epsilon^{abc} \epsilon^{a'b'c'} S_{u\gamma\delta}^{cc'}(\vec{x} + \vec{w}, 0) (\text{Tr}(S_u^{aa'}(\vec{x} + \vec{y}, 0) (C\gamma_5 S_d^{bb'}(\vec{x} + \vec{z}, 0) C\gamma_5)^T \\
&\quad + (C\gamma_5 S_d^{bb'}(\vec{x} + \vec{z}, 0) C\gamma_5)_{\gamma\alpha}^T S_{u\alpha\delta}^{aa'}(\vec{x} + \vec{y}, 0)_{\gamma\delta}), \tag{5}
\end{aligned}$$

where the required Wick contractions have been taken over the quark spinors, and  $S_u(\vec{x}, 0)$  and  $S_d(\vec{x}, 0)$  represent propagators for the  $u$  and  $d$  quarks respectively propagating from 0 to  $\vec{x}$ . A sum over  $\vec{x}$  is used to isolate the zero momentum state. Note that this definition of the wave function is not gauge invariant, and as such, gauge fixing is required. For large Euclidean times,

$$\sum_{\vec{x}} G_{\gamma\delta}(\vec{x}, \vec{y}, \vec{z}, \vec{w}, t) = \lambda_0 \lambda(\vec{y}, \vec{z}, \vec{w}) e^{-Mt} \left( \frac{1 + \gamma_0}{2} \right)_{\gamma\delta}, \tag{6}$$

where  $\lambda_0$  is the coupling of the source interpolator to the ground state of mass  $M$  (or energy  $E$  in the external field case) and  $\lambda(\vec{y}, \vec{z}, \vec{w})$  encapsulates information on the ground state wave function. Thus,  $G$  is directly proportional to the wave function. Through our use of gauge invariant Gaussian smearing at the source, the standard two point function as in Eq. (1) and the wave function at the source are gauge invariant.

### III. SIMULATION DETAILS

As this is the first investigation of the effects of a magnetic field on the wave function of the nucleon, we use an ensemble of 200 quenched configurations with a lattice volume of  $16^3 \times 32$ , generated using the Luscher-Weisz  $\mathcal{O}(a^2)$  improved gauge action [11]. The  $\mathcal{O}(a)$  improved FLIC (Fat-Link Irrelevant Clover) fermion action [12] is used to generate the quark propagators with fixed boundary conditions in the time direction. Four sweeps of stout link smearing [13] with smearing parameter  $\rho = 0.1$  are applied to the gauge links in the irrelevant operators of the FLIC action. We use  $\beta = 4.53$ , corresponding to a lattice spacing of  $a = 0.128$  fm, determined by the Sommer parameter,  $r_0 = 0.49$  fm [14]. We employ 50 sweeps of gauge invariant Gaussian smearing [15] to the fermion source at time slice 8. Two values for the hopping parameter are considered,  $\kappa = 0.12885$  and  $0.12990$ , corresponding to pion masses of 0.697 GeV and 0.532 GeV. The gauge fields generated are fixed to the Landau gauge

using the conjugate gradient Fourier acceleration method for improved actions [16], to an accuracy of 1 part in  $10^{12}$ .

The normalisation chosen for the wave function is to scale the raw correlation function data such that the sum (over  $\vec{x}$  and the parameter associated with the quark wave function coordinate) of the square of the correlation function is 1 for each Euclidean time,  $t$ . For the  $d$  quark, this is given by

$$\xi^2(t) \frac{1}{V} \sum_{\vec{z}, \vec{x}} G_{\gamma\delta}^*(\vec{x}, 0, \vec{z}, 0, t) G_{\gamma\delta}(\vec{x}, 0, \vec{z}, 0, t) = 1, \tag{7}$$

and similarly for the  $u$  quarks, with no sum over  $\gamma$  or  $\delta$ . Here,  $V$  is the spatial volume of the lattice. Note that the quark separation parameters  $d_1$  and  $d_2$  are zero here. The wave functions of other quark separations are then scaled by the same factor,  $\xi(t)$ . In reporting our results, we focus on the probability distribution,

$$\rho_{\gamma\delta} = \xi^2(t) \frac{1}{V} \sum_{\vec{x}} G_{\gamma\delta}^*(\vec{x}, \vec{y}, \vec{z}, \vec{w}, t) G_{\gamma\delta}(\vec{x}, \vec{y}, \vec{z}, \vec{w}, t). \tag{8}$$

For the zero field case, we report the probability distribution from the average of spin-up,  $(\gamma, \delta) = (1, 1)$  and spin down,  $(\gamma, \delta) = (2, 2)$  correlators. For finite  $\vec{B}$ , spin up and spin down probability distributions are reported individually. The time  $t$  is selected to lie well within the ground state dominant regime as identified by a standard covariance-matrix analysis of the local two-point function.

### IV. ZERO-FIELD RESULTS

We begin by looking at the probability distribution of the  $d$  quark with the aforementioned  $u$  quark separations in the Landau gauge. Immediately we notice that the probability distribution is not symmetric around the centre of mass of the proton. We note that in Fig. 1, the peak is centred around the  $u$  quark that resides in the scalar pairing with the  $d$  quark in Eq. (4). This leads

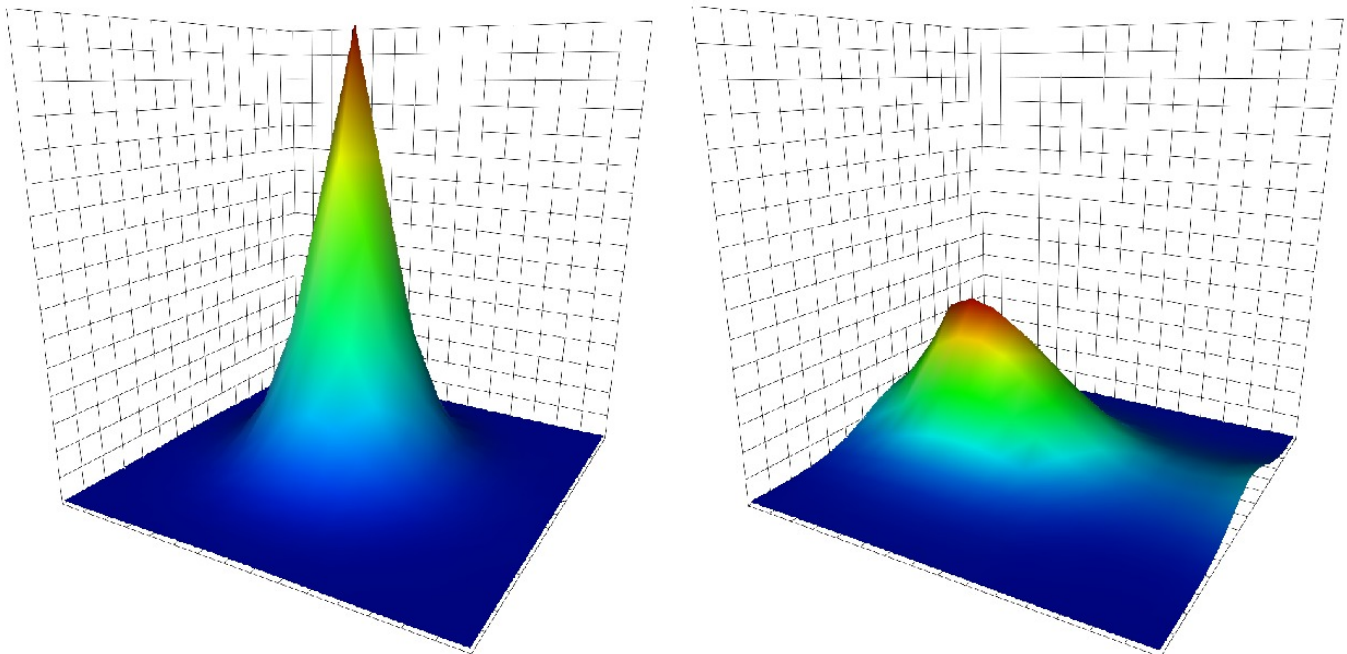


FIG. 1: (Colour Online) The Landau gauge probability distribution for the  $d$  quark of the proton from Eqs. (5) and (8), in the plane of the  $u$  quarks separated by zero lattice units (left), and by 7 lattice units (right). The  $d$  quark is seen to prefer to reside near the  $u$  quark which is placed in the scalar pair in the interpolating field of Eq. (4).

us to believe that the  $u$  and  $d$  quarks tend to form a scalar pair within the proton. At this point, we choose to anti-symmetrise the identical  $u$  quarks, changing our annihilation operator from Eq. (4) to

$$\chi_P(\vec{x}, \vec{y}, \vec{z}, \vec{w}) = \epsilon^{abc}(u_a^T(\vec{x} + \vec{y})C\gamma_5 d_b(\vec{x} + \vec{z}))u_c(\vec{x} + \vec{w}) + \epsilon^{abc}(u_a^T(\vec{x} + \vec{w})C\gamma_5 d_b(\vec{x} + \vec{z}))u_c(\vec{x} + \vec{y}). \quad (9)$$

This choice is motivated by the fact that the interpolating field places one of the  $u$  quarks permanently within the scalar pair, however, physically, this would not be the case, as the  $u$  quarks within the proton should be indistinguishable.

Upon implementing this symmetrisation, we see no evidence that diquark clustering is occurring at small  $u$ -quark separations. Rather, the probability distribution broadens and flattens around the centre of mass of the system. However, when we move to a separation of five or more lattice units, or 0.640 fm, we see the formation of two distinct peaks as illustrated in Fig. 2. At this stage, the  $u$  quarks are separated further than was considered in [4].

To more clearly illustrate this double peaked structure, we plot values of the probability distribution along the line joining the two fixed quarks in Fig. 3. We have taken advantage of correlations in the uncertainties in the lattice results and present the uncertainty relative to the value at  $x = 6$ .

In the Coulomb gauge, diquark clustering is present as

evidenced in the unsymmetrised wave function, however, the support in the centralized region hides the diquark clustering upon symmetrisation. Figure 2 illustrates results for  $u$  quarks separated by 7 lattice units. Such a difference in the probability distribution between the two gauges is a remarkable result.

In both the Landau and Coulomb gauges, the mass dependence of the probability distributions is almost negligible, as there are no significant differences in the shape of the probability distribution when the quark mass is changed. This was also noted in Refs. [1, 2]

When we look at the probability distribution of the scalar  $u$  quark (i.e. the  $u$  quark in the scalar pair with the  $d$  quark in Eq. 4) diquark clustering becomes more pronounced in the Landau gauge, as well as becoming apparent in the Coulomb gauge as illustrated in Fig. 4.

The probability distribution of the vector  $u$  quark (i.e. the  $u$  quark that carries the spinor index of  $\chi_P$  in Eq. (4)) in the Landau gauge also exhibits diquark clustering without a direct spin correlation in the interpolating field. Such a clustering is anticipated in constituent quark models with hyperfine interactions. Clustering is also observed in the Coulomb gauge. However, much like the  $d$  quark, the probability distribution is more towards the centre of mass of the system (Fig 5).

While it is possible to classify three types of quark probability distribution, including the  $d$  quark, scalar  $u$  quark and vector  $u$  quark probability distributions, the scalar  $u$  quark and vector  $u$  quark probability distributions are not physical quantities as the two  $u$  quarks in

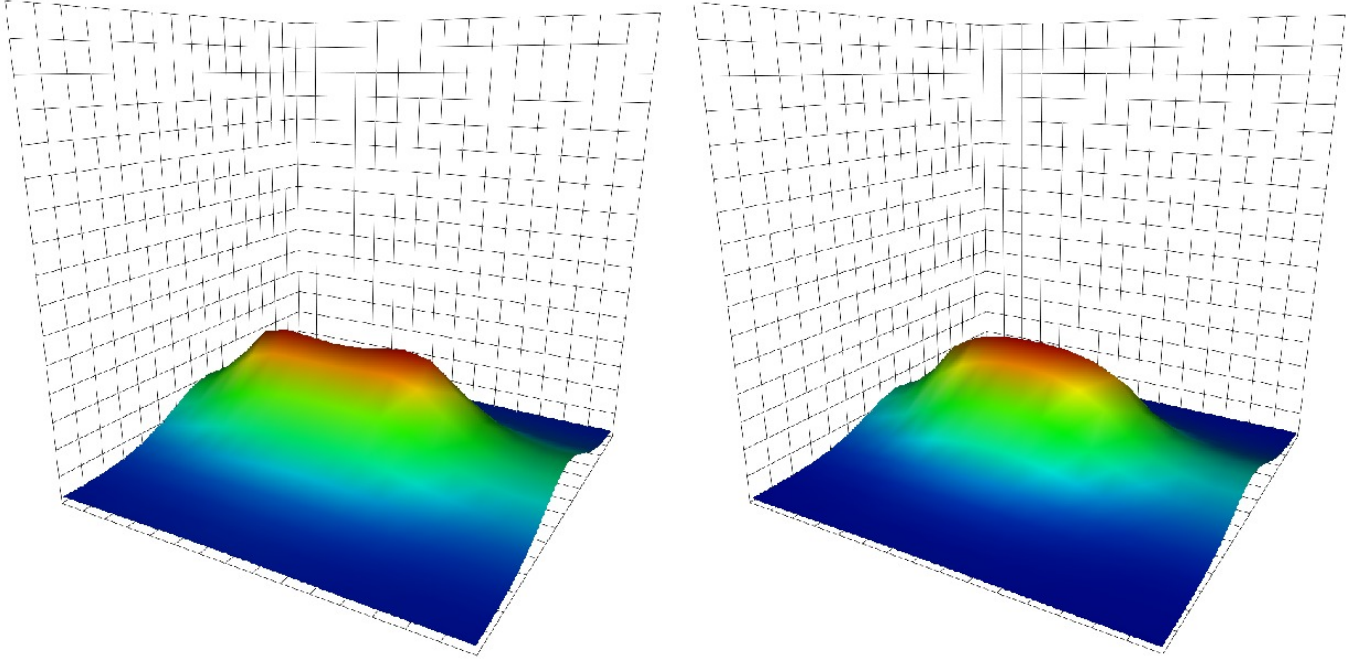


FIG. 2: (Colour Online) The probability distribution for the  $d$  quark of the proton in the plane of the  $u$  quarks separated by 7 lattice units, in the Landau gauge (left), and the Coulomb gauge (right). Two distinct peaks have formed over the location of the  $u$  quarks in the Landau gauge probability distribution, whereas a single, broad peak is visible over the centre of mass of the system in the Coulomb gauge. Note: as discussed following Eq. (7) the scale is such that the largest value of all of the fixed quark separations will sit at the top of the grid, with all other points of the probability distribution scaled accordingly.

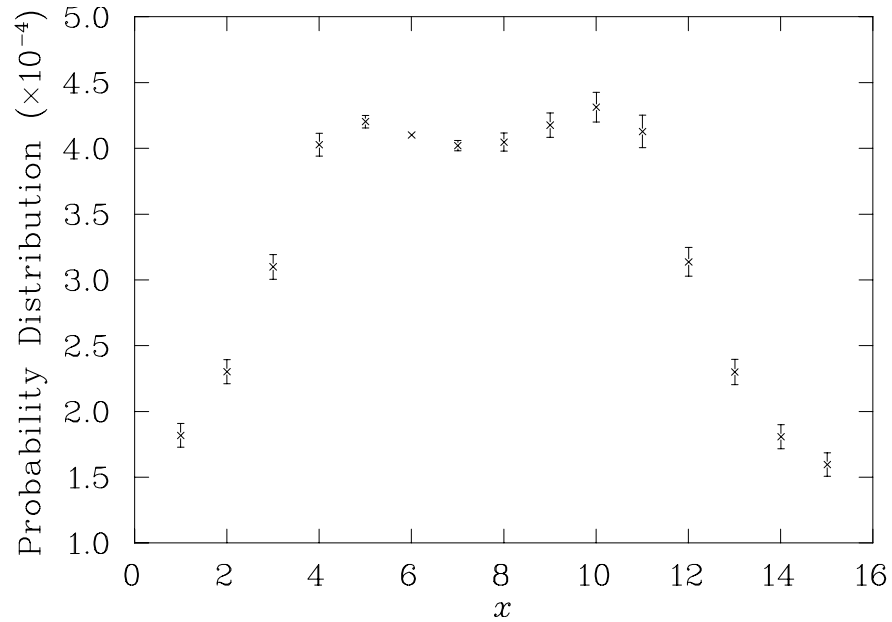


FIG. 3: The probability distribution of the  $d$  quark in the proton with the  $u$  quarks 7 lattice units apart along the  $x$  axis at  $x = 4$  and 11. To clearly display the double peak structure, uncertainties are reported relative to the distribution at  $x = 6$ .

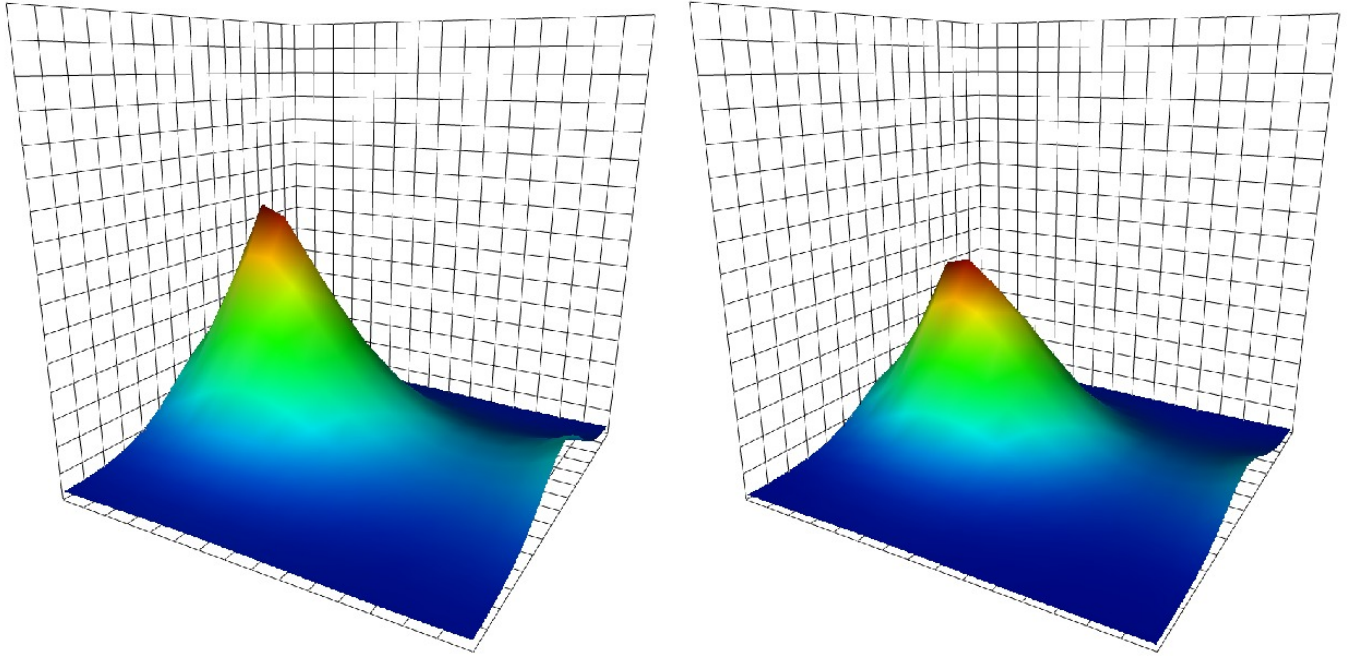


FIG. 4: (Colour Online) The probability distribution for the scalar  $u$  quark of the proton in the plane of the  $u$  and  $d$  quarks separated by 7 lattice units, in the Landau gauge (left), and the Coulomb gauge (right). In both gauges, the  $u$  quark is seen to prefer to be nearer the  $d$  quark. However, in the Coulomb gauge, the scalar  $u$  quark is closer to the centre of the lattice than in the Landau gauge probability distribution. The scale is as described in Fig. 2

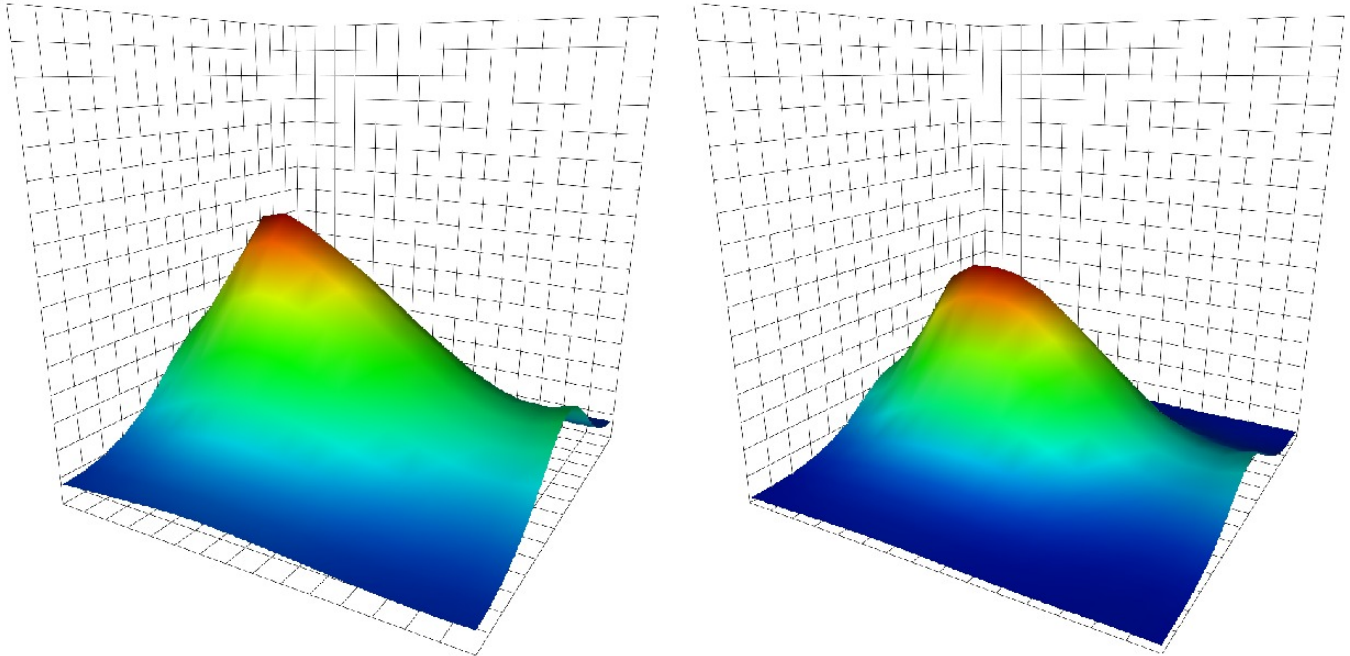


FIG. 5: (Colour Online) The probability distribution for the vector  $u$  quark of the proton in the plane of the  $u$  and  $d$  quarks separated by 7 lattice units, in the Landau gauge (left), and the Coulomb gauge (right). The probability distribution is similar to the  $d$  quark probability distribution in that strong clustering is seen in the Landau gauge. The Coulomb gauge results here reveal a small amount of preferred clustering with the  $d$  quark. Also of note is that these probability distributions show less structure than the others, as can be seen by the height of the smallest values, with the scale as described in Fig. 2

the proton are identical particles. The proper  $u$  quark probability distribution can be obtained from the same anti-symmetrised interpolating field of Eq. (9). In spite of the symmetrisation, the  $u$  quark allowed to vary prefers to reside near the  $d$  quark rather than the fixed  $u$  quark as illustrated in Fig. 6.

The probability distribution of the scalar  $u$  quark of Fig. 4 very closely resembles that of the symmetrised operator, indicating that the scalar term contributes the most to the symmetrised probability distribution of Fig. 6

We note that there are several reasons that we are able to see diquark clustering in the Landau gauge where Ref. [4] did not. Our use of a large smeared source, the averaging over  $\vec{x}$  in Eq. (5), using improved actions for both the quarks and the gauge fields and the consideration of hundreds of gauge fields provides better statistics, allowing access to further  $u$  quark separations with a high signal-to-noise ratio, as well as the ability to investigate lighter quark masses. Furthermore, our lattices extend twice as far in the temporal direction and use fixed boundary conditions, thus reducing the chance of any contamination associated with the boundary conditions.

Although models featuring diquarks within hadrons have been used extensively for many years [17], there has been little, if any, direct evidence for the existence of such a cluster within a particle. Earlier lattice studies that have paired two light quarks with a static quark [18, 19] have shown a large diquark ( $\mathcal{O}(1)$  fm) can form inside of a baryon, though with limited effect on the structure of the particle. More recently, light quarks have been paired with various diquark correlators [20] which suggest that diquarks are not a significant factor in light baryons. To the best of our knowledge, this is the first time that such a diquark configuration has been shown in a baryon composed of three light quarks.

## V. BACKGROUND FIELDS ON THE LATTICE

A background electromagnetic field can be added to the lattice in the form of a phase that multiplies the  $SU(3)$  links across the entire lattice. In this case, we wish to place a constant background magnetic field in the  $z$  direction, or  $\vec{B} = (0, 0, B)$ . In order to accomplish this we note that in the continuum  $B_z = \partial_x A_y^{EM} - \partial_y A_x^{EM}$ , where  $A^{EM}$  is a  $U(1)$  vector potential [5]. As such we need to modify this vector potential such that the magnetic field can remain constant across the periodic boundary conditions of the lattice. The definition of the plaquette in the  $xy$  plane at some point  $x$  is given by

$$W_{\mu\nu}^{EM}(x) = U_{\mu}^{EM}(x)U_{\nu}^{EM}(x+a\hat{\mu})U_{\mu}^{\dagger EM}(x+a\hat{\nu})U_{\nu}^{\dagger EM}(x), \quad (10)$$

where  $U_{\mu}^{EM}(x) = e^{iaeA_{\mu}(x)}$ , where  $a$  is the lattice spacing, and  $e$  is the electromagnetic coupling constant. Using a finite difference approximation to the derivative, this

becomes

$$W_{\mu\nu}^{EM}(x) = e^{ia^2 eF_{\mu\nu}(x)}. \quad (11)$$

Using the above definition for the magnetic field strength, our focus is on

$$W^{EM}(x) \equiv W_{xy}^{EM}(x) = -W_{yx}^{EM}(x) = e^{ia^2 eB}. \quad (12)$$

There are multiple vector potentials that allow such a field, two of which will be considered here. In the first of the two, we set  $U_y(x, y, z, t) = e^{iaeBx}$  and  $U_x(x, y, z, t) = 1$ . Away from the boundary of the lattice, this gives

$$\begin{aligned} W^{EM}(x, y, z, t) &= e^{iaeB(x+a)-iaeBx} \\ &= e^{ia^2 eB}, \end{aligned} \quad (13)$$

as required. On the boundary in the  $x$  direction, the periodic boundary conditions come into effect and the vector potential has to be modified in order that the field remains constant. This is accomplished by setting  $U_x(N_x, y, z, t) = e^{-iaeN_x B y}$ , where  $N_x$  is the extent of the lattice in the  $x$  direction, i.e. only on the boundary. The plaquette then becomes

$$\begin{aligned} W^{EM}(N_x, y, z, t) &= e^{iae(-N_x B y + B a + N_x B(y+a) - B N_x a)} \\ &= e^{ia^2 eB}, \end{aligned} \quad (14)$$

as required. On the corner of the  $xy$  plane, quantisation conditions for the field emerge

$$\begin{aligned} W^{EM}(N_x, N_y, z, t) &= e^{ia^2 B(-N_x N_y + 1 + N_x - N_x)} \\ &= e^{ia^2 eB} e^{-ia^2 e N_x N_y B}, \end{aligned} \quad (15)$$

where  $N_y$  is the extent of the lattice in the  $y$  direction. Hence, for the field to be constant at the corner of the lattice, it must be quantised such that

$$eB = \frac{2\pi n}{N_x N_y a^2}, \quad (16)$$

where  $n$  is a non-zero integer. The second method of placing a constant magnetic field on the lattice used here is to set  $U_y = 1$  and  $U_x = e^{-iaeB y}$  away from the boundary and setting  $U_y = e^{iaeN_y B x}$  for  $x = (x, N_y, z, t)$ . This implementation has the same quantisation conditions as in Eq. (16).

There are several points to note about placing a background field on the lattice, the first of which is that adding any constant to the potential will not affect the resultant field. It can also be shown that there is a gauge transformation that links both of the above implementations of the background field, given by,

$$G(x, y) = e^{ieBxy}, \quad (17)$$

where  $x, y$  denote lattice sites  $1, 2, \dots, N_x, N_y$  in units of the lattice spacing  $a$  and

$$U_{\mu}(x) \rightarrow G(x)U_{\mu}(x)G^{\dagger}(x+\hat{\mu}). \quad (18)$$

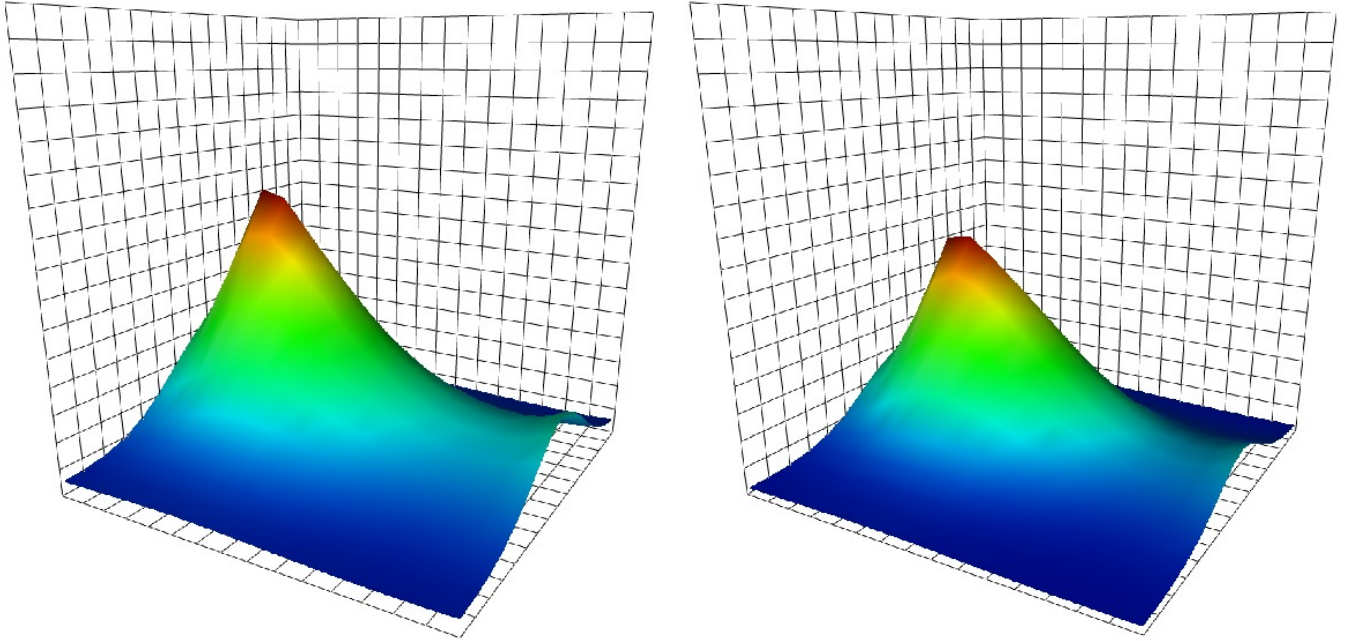


FIG. 6: (Colour Online) The probability distribution for an anti-symmetrised  $u$  quark of the proton in the plane of the remaining quarks which are separated by 7 lattice units, in the Landau gauge (left), and the Coulomb gauge (right). In contrast to the  $d$  quark probability distribution, a single peak is visible above the location of the  $d$  quark in both the Coulomb and the Landau gauge. Note: as discussed following Eq. (7) the scale is such that the largest value of all of the fixed quark separations will sit at the top of the grid, with all other points of the probability distribution scaled accordingly.

These implementations of the background field are applied to both the Landau and Coulomb-fixed configurations.

We expect that this magnetic field will cause a distortion of the probability distribution, as the proton responds to the presence of the field. Since the magnetic field is in the  $z$  direction, we expect that physical distortion will be symmetric about this direction, and all other effects will be a result of the choice of the gauge potential  $\vec{A}$ .

A particle on the lattice in the presence of a background magnetic field will undergo a mass shift given by

$$m(\vec{B}) = m(0) + \frac{|e\vec{B}|}{2m} + \mu \cdot \vec{B} + \frac{1}{2}\beta_m B^2, \quad (19)$$

where  $\mu$  is the magnetic moment of the particle and  $\beta_m$  is the magnetic polarisability [6]. Because of the quantisation imposed by the periodic boundary conditions, the magnetic field will be very large. For  $n = 3$ , required to accommodate the fractional charges, the value of the field on our lattices is  $eB = 0.175 \text{ GeV}^2$ , which implies that the first order response of a proton to the field would be  $\mu B = 260 \text{ MeV}$  in the continuum. On the lattice however, the mass of the ground state of the proton is larger and the moment itself is smaller[8], and as such the response will be smaller at approximately 150 MeV at our lighter mass.

## VI. BACKGROUND MAGNETIC FIELD RESULTS

The first notable result from the use of the aforementioned method of placing a background field on the lattice is that an asymmetry is produced in the direction of the changing vector potential as illustrated in Fig. 7. This asymmetry occurs in both the Landau gauge and Coulomb gauge to a similar extent. This is an unphysical result of the gauge-dependent method in which we place the field on the lattice, which can be shown by using the second implementation described in Sec. V. Upon doing this, the asymmetry in the probability distribution can be seen to move to the direction of the vector potential once again as shown in Fig. 7. In order to minimise the effect of the choice of the gauge potential on the probability distribution, we choose an average over four implementations of the background field: the two implementations described above and two in which a gauge transformation is applied such that the magnitude of the vector potential decreases across the lattice. For the first implementation

$$G(x, y) = e^{iaeBN_{xy}}, \quad (20)$$

and similarly for the second of the two implementations. Once averaging over the four vector potentials has been

applied, symmetry around the  $z$  axis is obtained. Thus, we look at the probability distribution in the  $xz$  plane.

In spite of the very large magnetic field strength imposed by the boundary conditions, the change in the probability distribution is quite small for the case where the remaining quarks are both located in the centre of the lattice, (Fig. 8). This subtle result is consistent with that expected from the polarisability as the current experimental value for the proton polarisability is  $\beta_M = 1.9(5) \times 10^{-4} \text{ fm}^3$  which gives the second order response to the field of around,  $\frac{1}{2}\beta_M e^2 B^2 = 0.4 \text{ MeV}$ .

Very little spin dependence can be seen in the probability distributions themselves, the probability distributions of the spin up proton quarks are largely the same as the probability distributions of the spin down proton. A subtle difference appears in the vector  $u$  quark probability distributions in the Coulomb gauge, as illustrated in Fig. 9. A more prominent difference is visible in the Landau gauge (Fig. 10). The probability distribution appears more spherical and localized when the spin is aligned with the field, and a very subtle asymmetry is present in the direction of the field. Spin dependence also manifests itself in the energy of the proton, as can be seen in Table I, where the energy of the proton when its spin is anti-aligned to the field is lower than the zero-field energy, indicating that Landau levels are not having a dominant effect on the particle energy. The spin aligned proton receives a larger energy, due to the sign on the moment term.

TABLE I: The dependence of the spin up and spin down mass of the proton on the background magnetic field. When the spin is aligned with the field (up), the mass of the proton increases, whereas when the spin is anti-aligned with the field (down), we see a mass decrease.

$\kappa$	spin	$B$	Mass (GeV)	$m_\pi^2$ (GeV <sup>2</sup> )	window	$\chi^2/dof$
0.12885	averaged	0	1.492(10)	0.486	10-18	1.001
	down	-3	1.366(11)		10-14	0.879
	up	-3	1.688(11)		10-18	0.991
0.12990	averaged	0	1.327(11)	0.283	10-18	0.954
	down	-3	1.197(13)		10-14	1.061
	up	-3	1.528(13)		10-15	0.983

The localization of the spin aligned probability distribution can be understood in terms of a constituent quark mass effect in a simple potential model. The effect of the increased proton energy is to cause an increase in the constituent quark mass, hence causing the probability distribution to sit lower in the potential. This makes the spin aligned probability distribution smaller than the spin anti-aligned probability distribution.

As the quarks are separated, the probability distributions in the background field tend to be more localized than the same probability distributions without a background field. Some stretching along the field orientation at the centre of the distribution is apparent, making the distribution more spherical (Fig. 11). This is consistent with the effect of raising the constituent quark mass. In

the Landau gauge, the diquark clustering is removed from the  $d$  quark probability distribution by the presence of the field as illustrated in Fig. 12.

In contrast, diquark clustering is still apparent in the  $u$  quark probability distribution in the presence of the field, with the distribution moving towards the centre of the baryon on application of the magnetic field, as shown in Figs. 13 and 14. The scalar  $u$  quark probability distribution also shows more localization than either the vector  $u$  quark or  $d$  quark probability distributions. The anti-symmetrised  $u$  quark probability distribution illustrated in Figs. 15 and 16 still bears close resemblance to that of the scalar  $u$  quark. However, it is not as localized as the scalar  $u$  quark probability distribution due to the contribution from the vector  $u$  quark required to anti-symmetrise the identical  $u$  quarks. The Landau gauge probability distribution is still larger than the Coulomb gauge probability distribution.

As illustrated in Figs. 17 and 18 for the Coulomb and Landau gauges respectively, the effect of the field on the probability distribution of the vector  $u$  quark is more pronounced than the  $d$  quark and scalar  $u$  quark probability distributions.

The spin orientation dependence as the quarks are separated remains largely the same as in the case where the quarks are at the origin, with the vector  $u$  quark probability distribution changing the most between the spin aligned and anti-aligned cases. In the case where the spin is aligned with the field and the mass increases, the probability distribution becomes more localized perpendicular to the field relative to when the spin is anti-aligned with the field. This is in keeping with the constituent quark model, where the field causes the constituent quark mass to increase, and as such, the proton sits lower in the potential.

Very little spin dependence is visible in the  $d$  quark and scalar  $u$  quark probability distributions. However, the effect on the probability distribution due to the magnetic field is more prominent when the remaining quarks are separated, compared to when the quarks are at the origin.

## VII. CONCLUSION

In this study, we have performed the first examination of the probability distribution of quarks in the proton in the presence of a background magnetic field in both the Landau and Coulomb gauges.

We have shown that there is a distinct difference between the  $d$  quark probability distributions in the Landau and Coulomb gauge, with the Landau gauge exhibiting clear diquark clustering. The probability distributions in the Coulomb gauge did not. The scalar  $u$  quark and vector  $u$  quark probability distributions show clear diquark clustering in both the Landau and Coulomb gauge, with the scalar  $u$  quark being more tightly bound to the  $d$  quark than the vector  $u$  quark probability distribution. This is the first direct evidence of the ability of a scalar



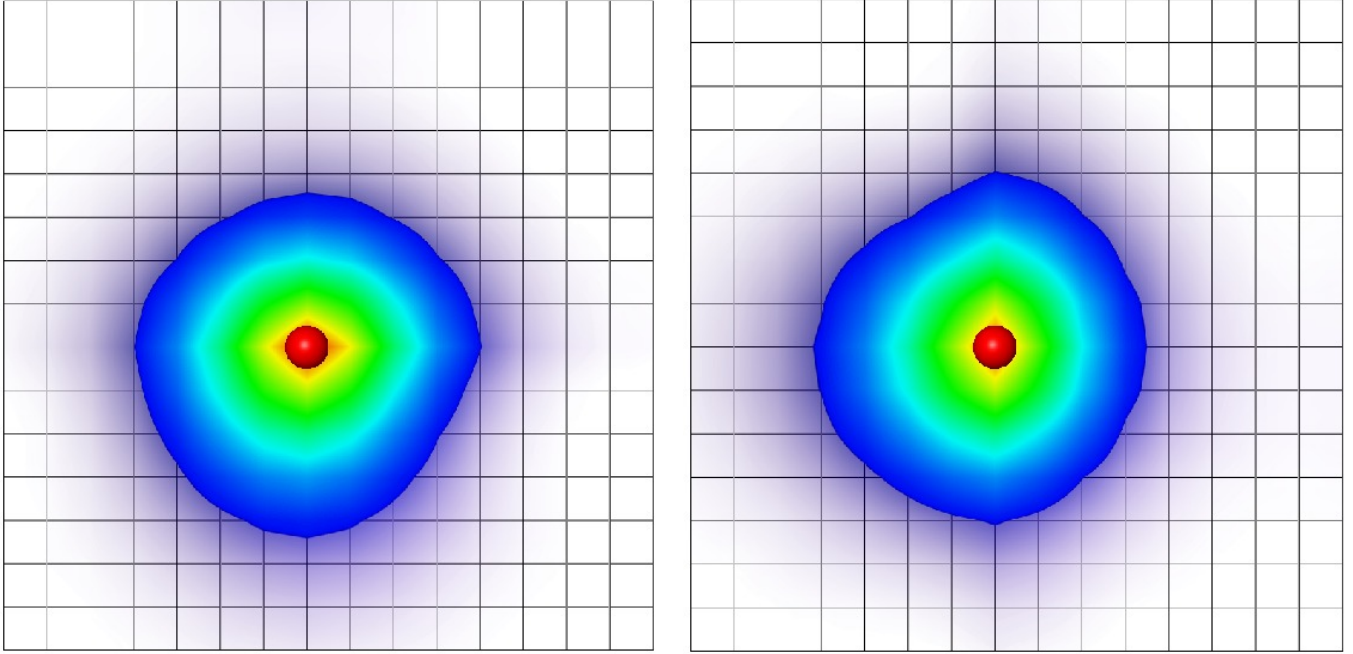


FIG. 7: (Colour online) The probability distribution for the  $d$  quark cut in the  $x - y$  plane of the  $u$  quarks, in the presence of a background magnetic field in the Landau gauge, with the first implementation (left), and the second implementation (right) of the vector potential described in Sec. V. In this image, the field,  $\vec{B}$ , is pointing into the page. The red sphere denotes the location of the remaining quarks. There is a clear asymmetry perpendicular to the field that changes with the vector potential,  $A_\mu$ , in spite of the background magnetic field not changing.

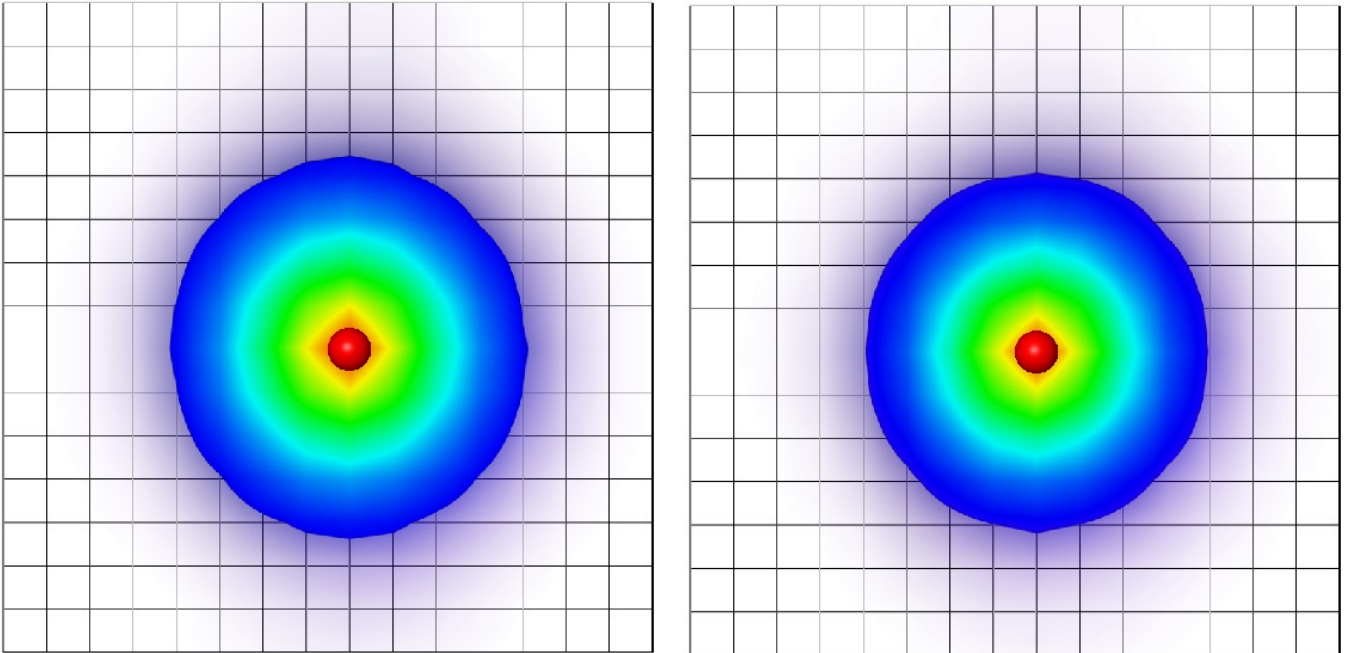


FIG. 8: (Colour online) The probability distribution for the  $d$  quark cut in the  $x - z$  plane of the  $u$  quarks, after symmetrising the vector potential,  $A_\mu$  in the presence of the field in the Landau gauge (left) and Coulomb gauge (right). In this image, the field,  $\vec{B}$ , is pointing to the top of the page, and the  $u$  quarks are both in the centre of the lattice, denoted by the red sphere. In spite of the magnitude of the field, a fairly small deviation from spherical symmetry is seen in both gauges.

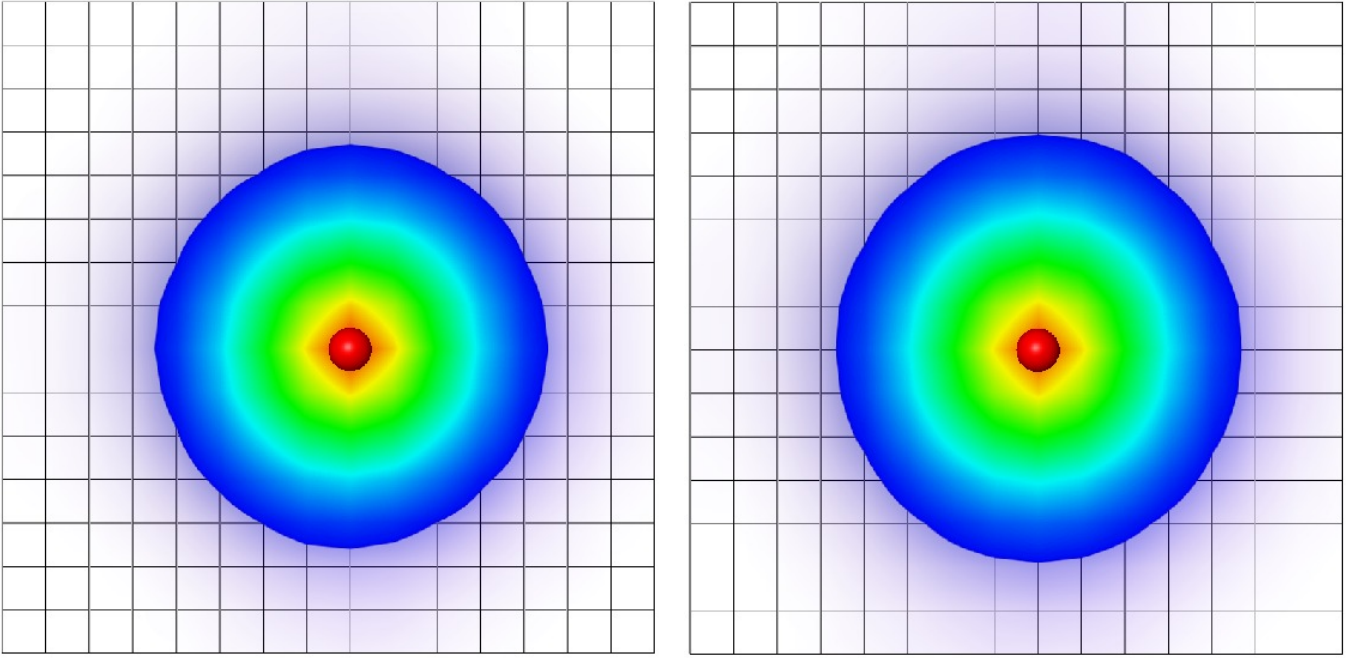


FIG. 9: (Colour online) The probability distribution for the vector  $u$  quark in the presence of the background field, cut in the  $x - z$  plane of the remaining quarks in the Coulomb gauge with the spin aligned (left) and anti-aligned (right) to the field. The direction of the field is down the page, and the red sphere denotes the remaining quarks. The probability distribution appears more spherical and localized when aligned with the field, and a very subtle asymmetry is present in the direction of the field. The smallest value shown for both probability distributions is 10% of the peak value.

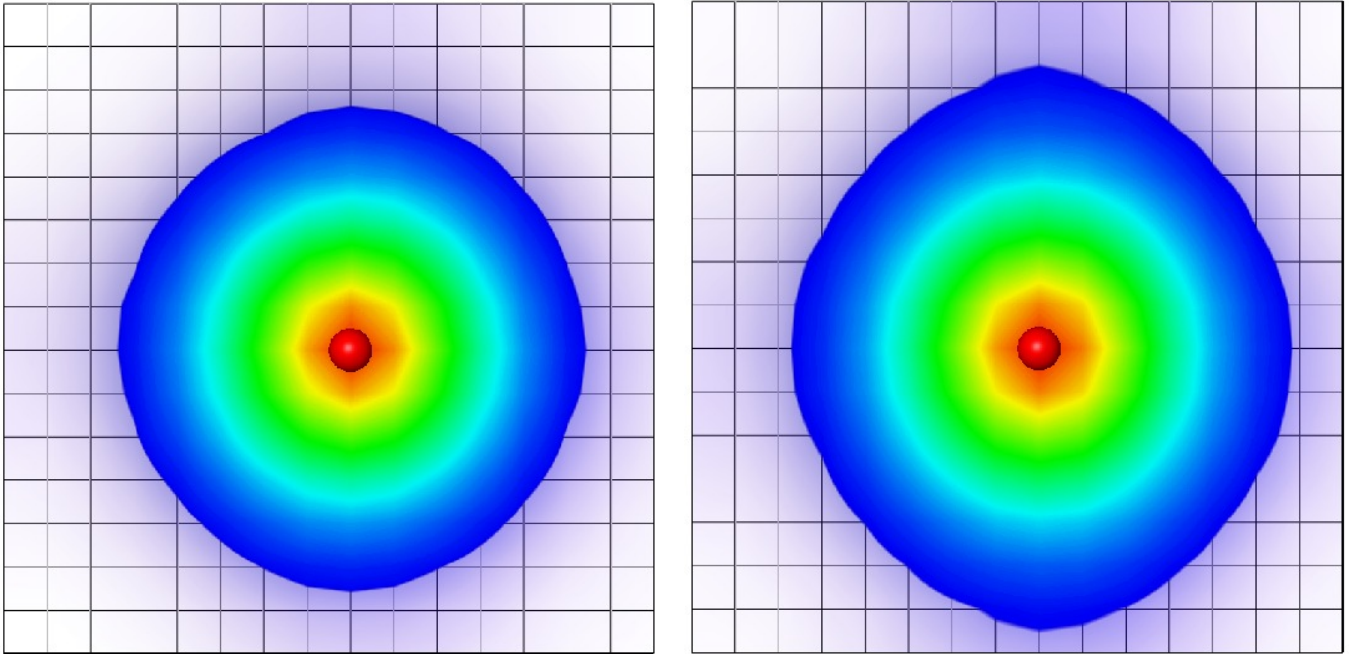


FIG. 10: (Colour online) The probability distribution of the vector  $u$  quark in the presence of the background field, cut in the  $x - z$  plane of the remaining quarks in the Landau gauge with the spin aligned (left) and anti-aligned (right) to the field, and the red sphere denotes the remaining quarks. The direction of the field is down the page. Much like in the Coulomb gauge, the probability distribution appears more spherical and localized when aligned with the field. The smallest value shown for both probability distributions is 10% of the peak value.

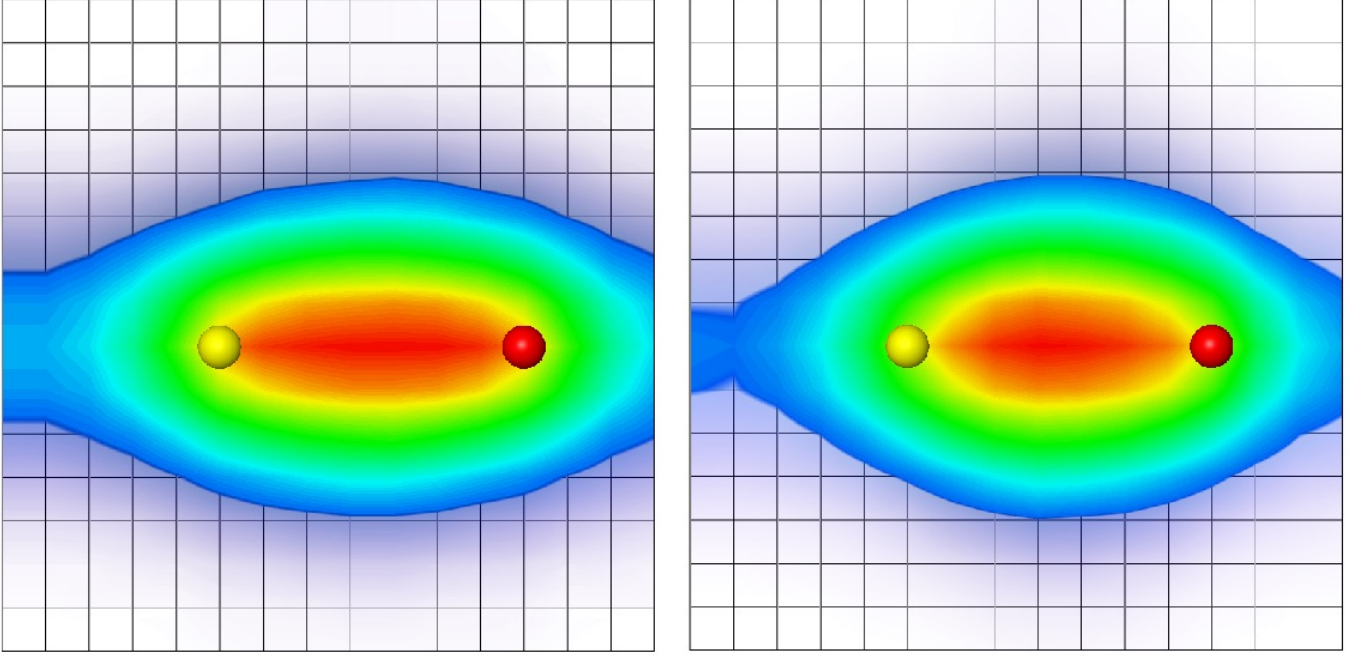


FIG. 11: (Colour online) The probability distribution of the  $d$  quark in the Coulomb gauge cut in the  $x-z$  plane of the  $u$  quarks which are separated by seven lattice units in the transverse direction with zero background field (left) and in the presence of the field (right). The direction of the field is up the page and the spheres denote the positions of the  $u$  quarks. The smallest value shown for both probability distributions is 20% of the peak value.

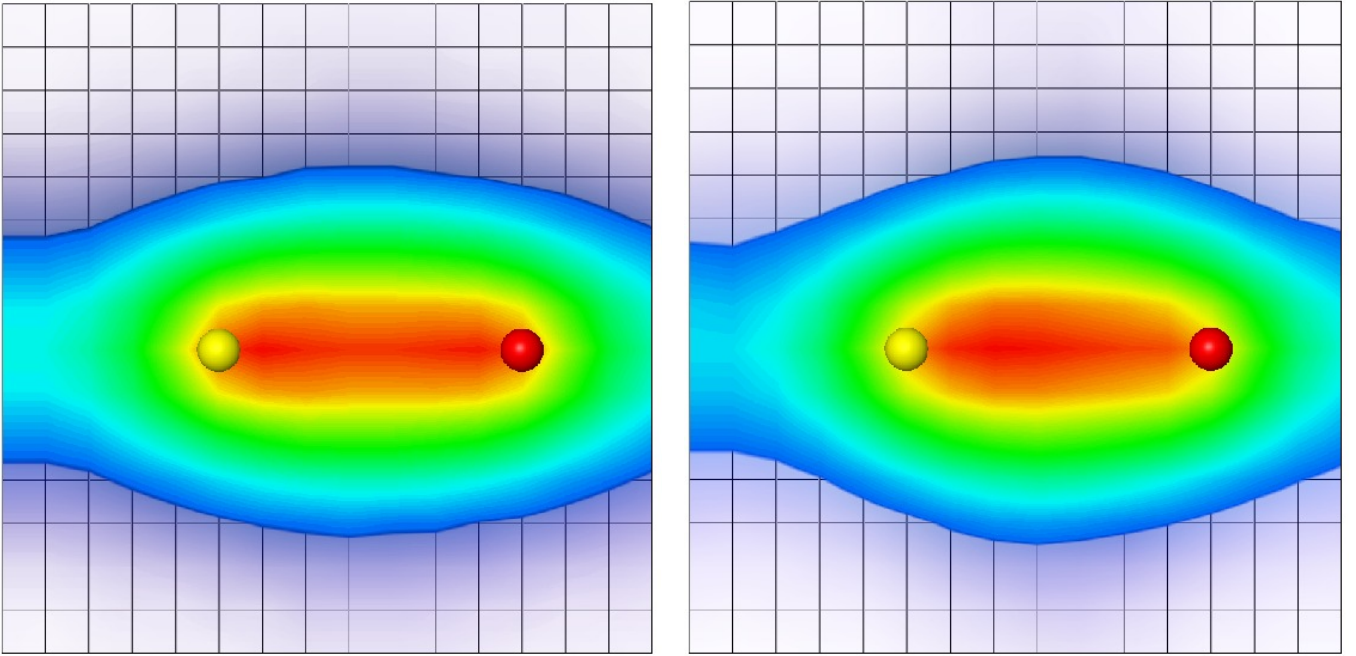


FIG. 12: (Colour online) The probability distribution of the  $d$  quark, in the Landau gauge cut in the  $x-z$  plane of the remaining quarks which are separated by 7 lattice units in the transverse direction with zero background field (left) and in the presence of the field (right). The spheres denote the positions of the  $u$  quarks. The diquark clustering is barely visible in this view, and disappears completely in the presence of the field. The probability distributions are broader in the Landau gauge and the smallest value shown for both probability distributions is 20% of the peak value.

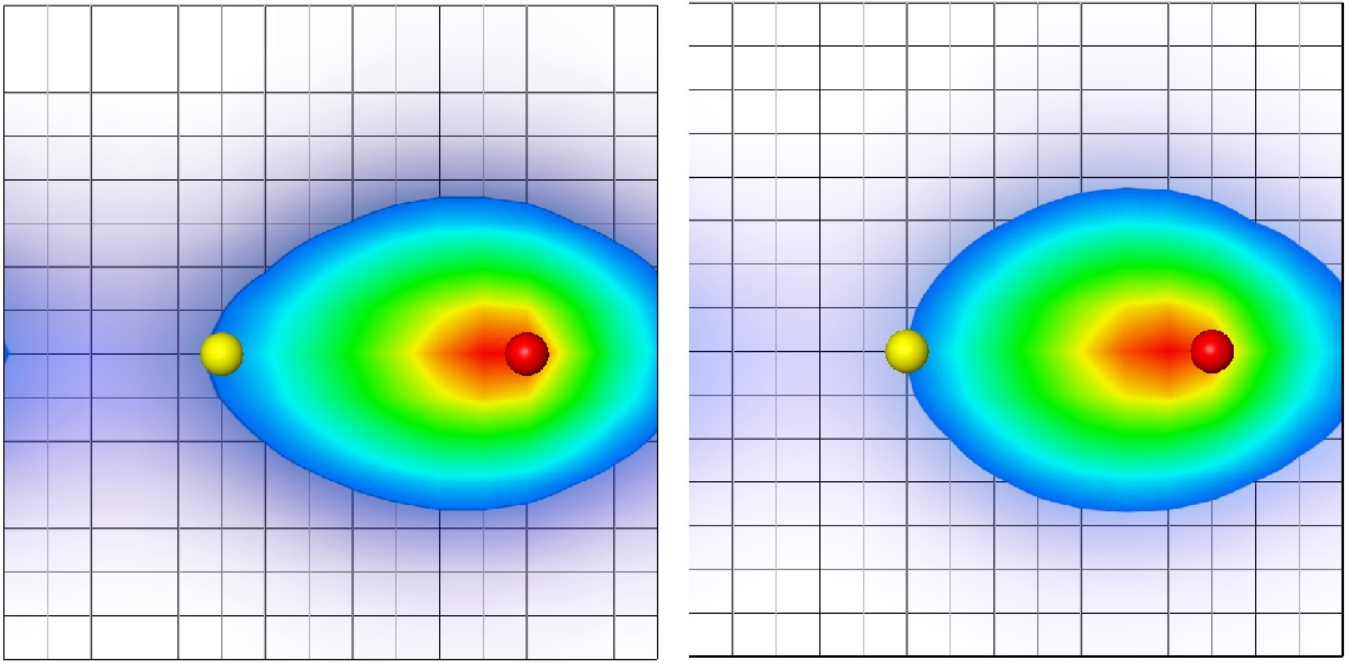


FIG. 13: (Colour online) The probability distribution of the scalar  $u$  quark in the Coulomb gauge cut in the  $x - z$  plane of the remaining quarks which are separated by seven lattice units in the transverse direction with zero background field (left) and in the presence of the field (right). The direction of the field is up the page and the  $d$  quark is on the right, denoted by the red sphere. In contrast to the  $d$  quark probability distribution, there is still a distinct preference for the formation of a scalar diquark. When the field is applied, the probability distribution can be seen to move toward the centre of the lattice. The smallest value shown for both probability distributions is 20% of the peak value.

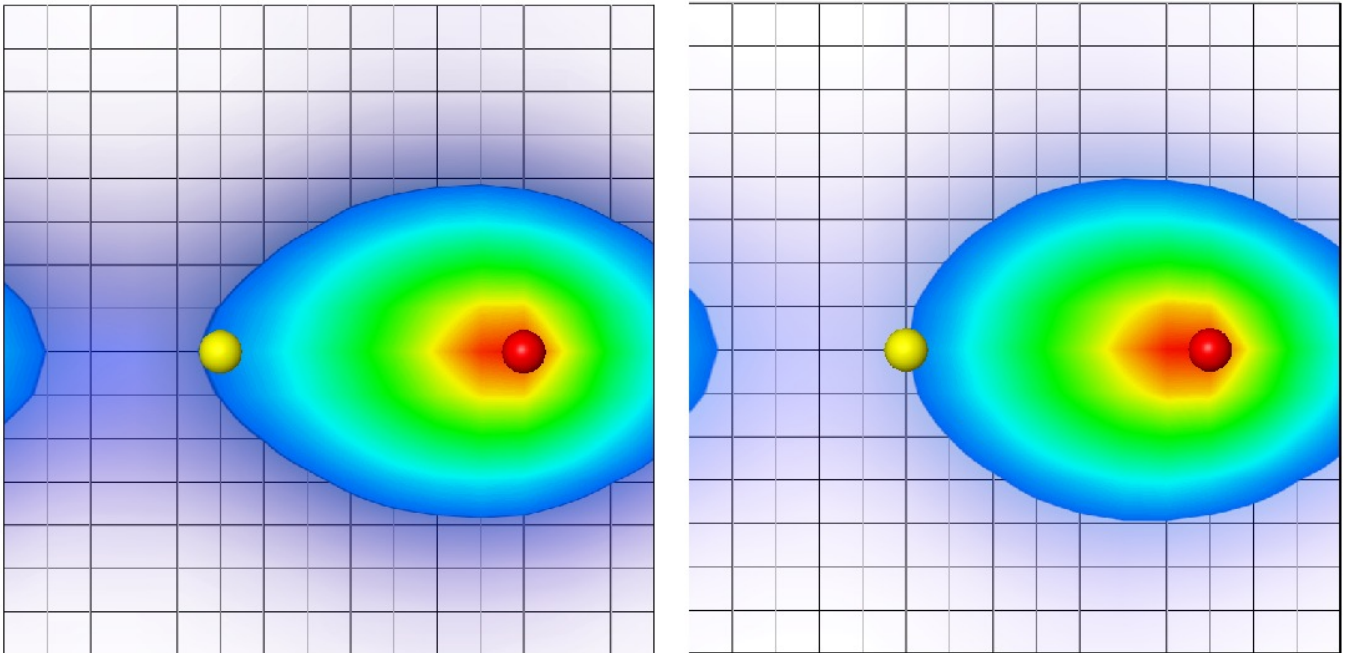


FIG. 14: (Colour online) The probability distribution of the scalar  $u$  quark, in the Landau gauge which are separated by 7 lattice units in the transverse direction with zero background field (left) and in the presence of the field (right). The direction of the field is up the page and the  $d$  quark is on the right, denoted by the red sphere. Preference towards the centre of the lattice is also visible in the Landau gauge, but is more subtle than in the Coulomb gauge. The probability distributions are broader in the Landau gauge and the smallest value shown for both probability distributions is 20% of the peak value.

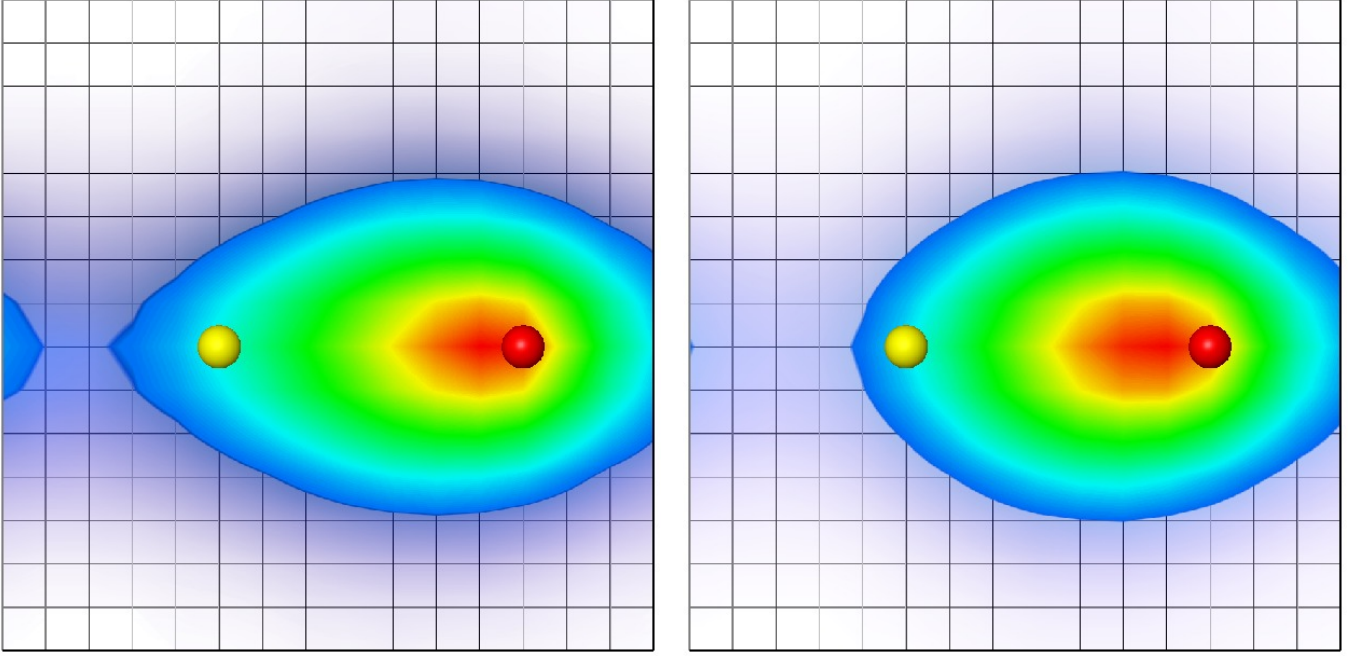


FIG. 15: (Colour online) The probability distribution of a  $u$  quark in the Coulomb gauge cut in the  $x - z$  plane of the remaining quarks which are separated by seven lattice units in the transverse direction with zero background field (left) and in the presence of the field (right). The direction of the field is up the page and the  $d$  quark is on the right, denoted by the red sphere. The symmetrised  $u$  quark probability distribution bears close resemblance to the scalar  $u$  quark, but less is localized due to the vector  $u$  quark contribution. The smallest value shown for both probability distributions is 20% of the peak value.

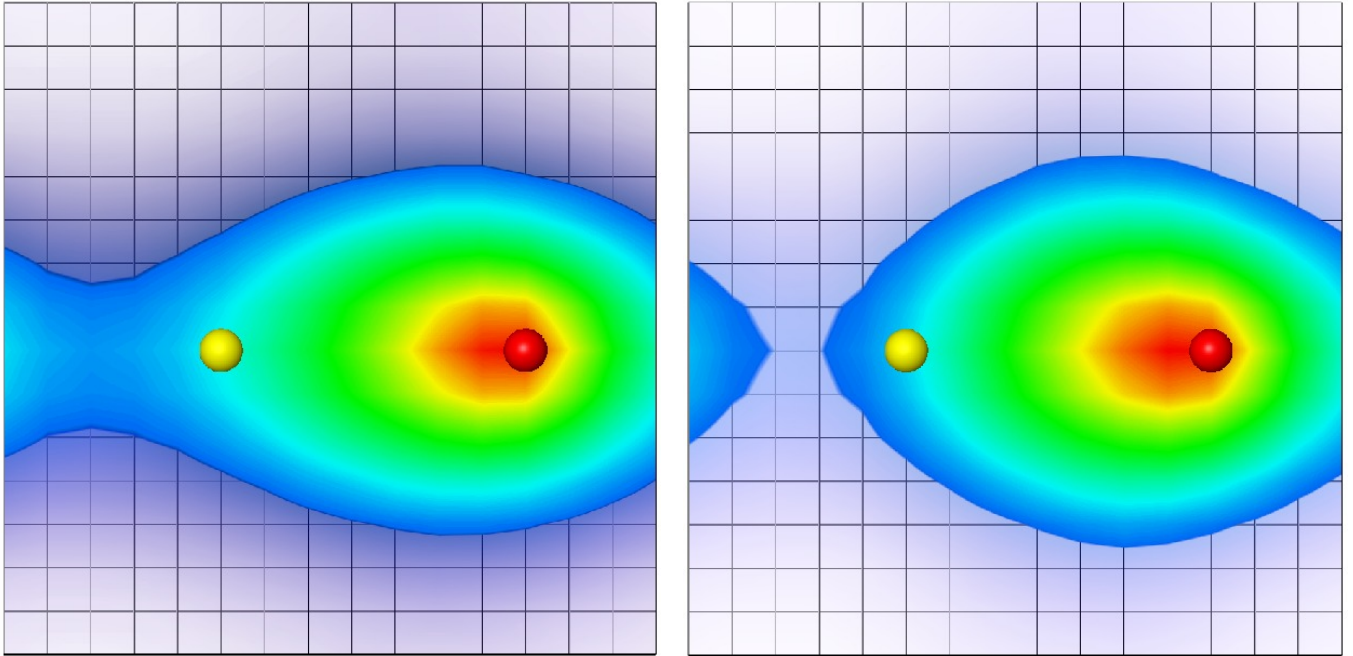


FIG. 16: (Colour online) The probability distribution of a  $u$  quark, in the Landau gauge cut in the  $x - z$  plane of the remaining quarks which are separated by 7 lattice units in the transverse direction with zero background field (left) and in the presence of the field (right). The direction of the field is up the page and the  $d$  quark is on the right, denoted by the red sphere. The contribution to the symmetrised probability distribution from the vector  $u$  quark is enhanced in the Landau gauge compared to the Coulomb gauge. The smallest value shown for both probability distributions is 20% of the peak value.

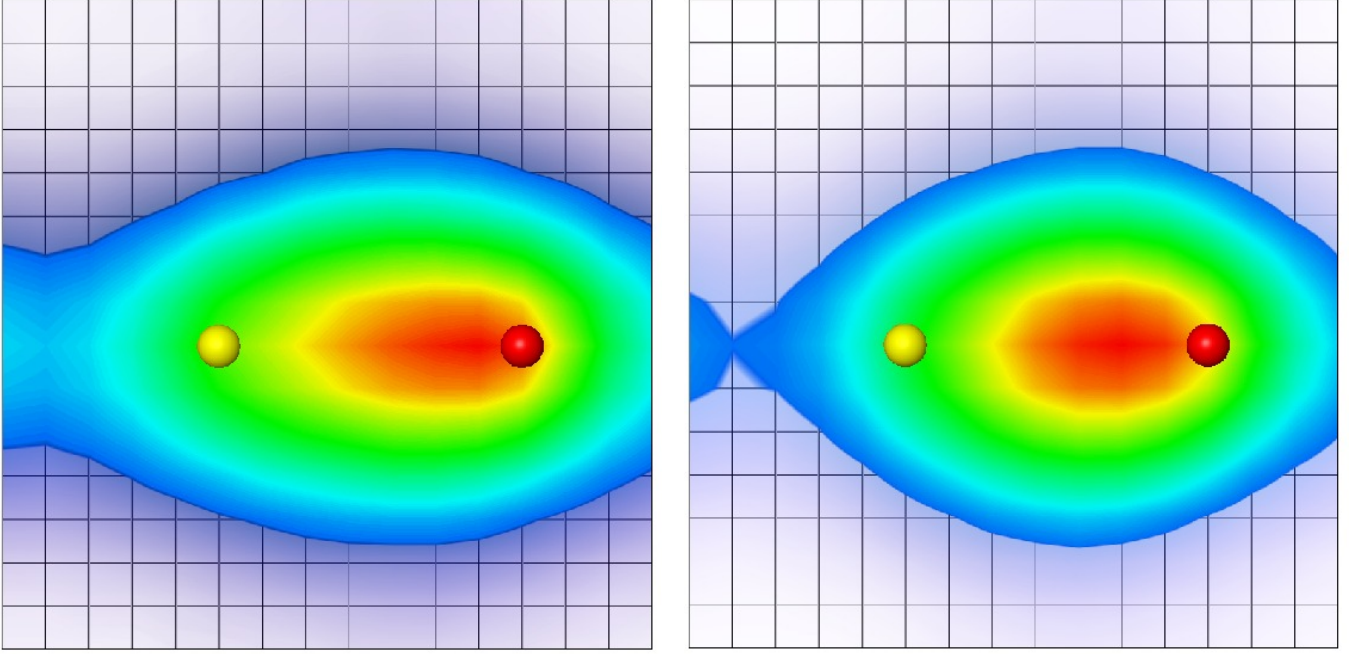


FIG. 17: (Colour online) The probability distribution of the vector  $u$  quark in the Coulomb gauge cut in the  $x - z$  plane of the remaining quarks which are separated by seven lattice units in the transverse direction with zero background field (left) and in the presence of the field (right). The direction of the field is up the page and the  $d$  quark is on the right, denoted by the red sphere. The effect of the field on the vector  $u$  quark probability distribution is more pronounced than the  $d$  quark and scalar  $u$  quark probability distributions. The smallest value shown for both probability distributions is 20% of the peak value.

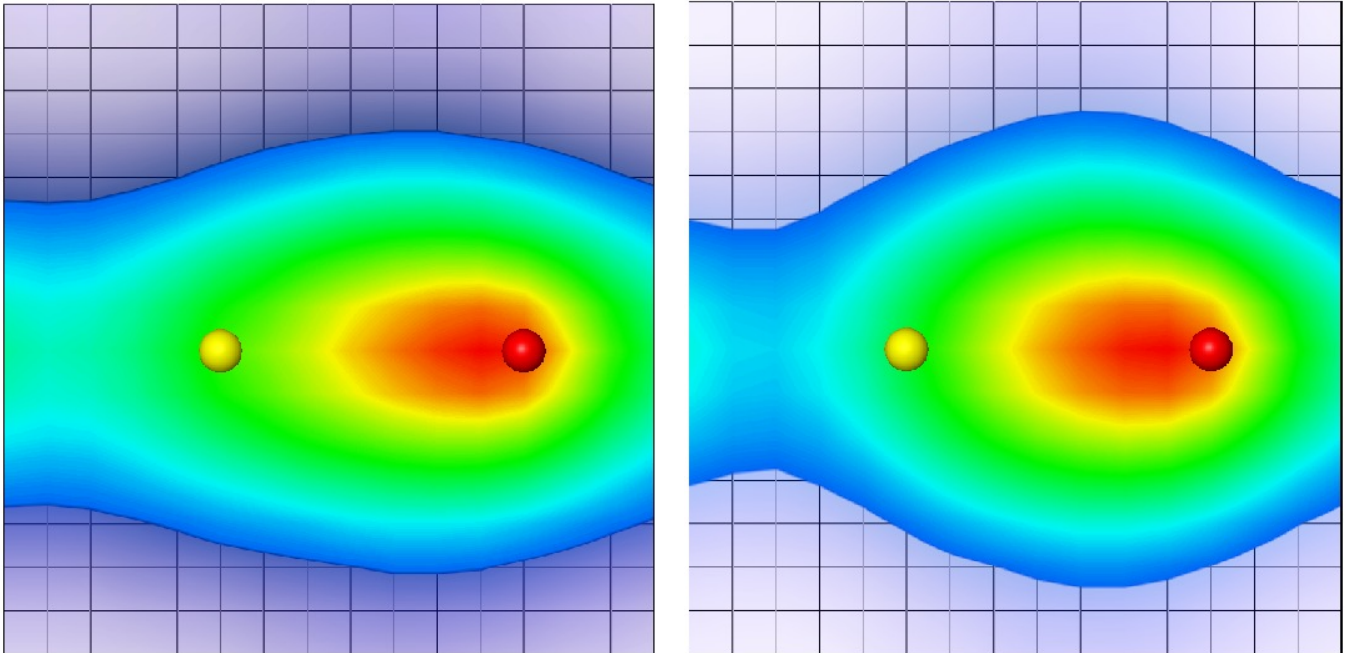


FIG. 18: (Colour online) The probability distribution of the vector  $u$  quark, in the Landau gauge cut in the  $x - z$  plane of the remaining quarks which are separated by 7 lattice units in the transverse direction with zero background field (left) and in the presence of the field (right). The direction of the field is up the page and the  $d$  quark is on the right, denoted by the red sphere. The smallest value shown for both probability distributions is 20% of the peak value.

diquark pair to form in a baryon. Also, the probability distributions in the Landau gauge were larger than those in the Coulomb gauge.

On the application of the background field, we found a gauge dependence in the probability distribution in the direction of the vector potential. A symmetrisation was performed to rectify this.

In spite of the very large magnetic field required by the quantisation conditions, the change in the probability distribution is small, being most prominent in the vector  $u$  quark. The effect is to elongate the distribution along the axis of the field while generally localizing the distribution. The vector  $u$  quark exhibits the most spin dependence, with the probability distribution being more localized when the spin is aligned with the magnetic field. This effect can be understood in terms of a constituent quark model where the constituent quark mass increases in the presence of the magnetic field.

More notable spin dependence appeared in the energy

of the proton itself, largely associated with the magnetic moment, as opposed to higher order effects impacting the structure of the proton. As the nucleon is rather stiff and only slightly more localized in a magnetic field, we anticipate the background field approach to determining the magnetic moment of baryons to be effective, even in a strong background field.

## Acknowledgments

This research was undertaken on the NCI National Facility in Canberra, Australia, which is supported by the Australian Commonwealth Government. We also thank eResearch SA for generous grants of supercomputing time which have enabled this project. This research is supported by the Australian Research Council.

- 
- [1] B. Velikson and D. Weingarten, Nucl. Phys. B **249**, 433 (1985).
  - [2] M. C. Chu, M. Lissia and J. W. Negele, Nucl. Phys. B **360**, 31 (1991).
  - [3] R. Gupta, D. Daniel and J. Grandy, Phys. Rev. D **48** (1993) 3330 [arXiv:hep-lat/9304009].
  - [4] M. W. Hecht and T. A. DeGrand, Phys. Rev. D **46**, 2155 (1992).
  - [5] J. Smit and J. C. Vink, Nucl. Phys. B **286**, 485 (1987).
  - [6] G. Martinelli, G. Parisi, R. Petronzio and F. Rapuano, Phys. Lett. B **116**, 434 (1982).
  - [7] C. W. Bernard, T. Draper, K. Olynyk and M. Rushton, Phys. Rev. Lett. **49**, 1076 (1982).
  - [8] F. X. Lee, R. Kelly, L. Zhou and W. Wilcox, Phys. Lett. B **627**, 71 (2005) [arXiv:hep-lat/0509067].
  - [9] M. Burkardt, D. B. Leinweber and X. m. Jin, Phys. Lett. B **385** (1996) 52 [arXiv:hep-ph/9604450].
  - [10] F. X. Lee, L. Zhou, W. Wilcox and J. C. Christensen, Phys. Rev. D **73**, 034503 (2006) [arXiv:hep-lat/0509065].
  - [11] M. Luscher and P. Weisz, Commun. Math. Phys. **97**, 59 (1985) [Erratum-ibid. **98**, 433 (1985)].
  - [12] J. M. Zanotti, D. B. Leinweber, W. Melnitchouk, A. G. Williams and J. B. Zhang, Lect. Notes Phys. **663**, 199 (2005) [arXiv:hep-lat/0407039].
  - [13] C. Morningstar and M. J. Peardon, Phys. Rev. D **69**, 054501 (2004) [arXiv:hep-lat/0311018].
  - [14] R. Sommer, Nucl. Phys. B **411**, 839 (1994) [arXiv:hep-lat/9310022].
  - [15] S. Gusken, Nucl. Phys. Proc. Suppl. **17**, 361 (1990).
  - [16] C. T. H. Davies *et al.*, Phys. Rev. D **37**, 1581 (1988).
  - [17] M. Anselmino, E. Predazzi, S. Ekelin, S. Fredriksson and D. B. Lichtenberg, Rev. Mod. Phys. **65**, 1199 (1993).
  - [18] C. Alexandrou, P. de Forcrand and B. Lucini, PoS **LAT2005**, 053 (2006) [arXiv:hep-lat/0509113].
  - [19] C. Alexandrou, Ph. de Forcrand and B. Lucini, Phys. Rev. Lett. **97**, 222002 (2006) [arXiv:hep-lat/0609004].
  - [20] T. DeGrand, Z. Liu and S. Schaefer, Phys. Rev. D **77**, 034505 (2008) [arXiv:0712.0254 [hep-ph]].